Synthesis and properties of Fe_3O_4 nanofibers and nanoribbons via electrospinning

QIANLI MA, JINXIAN WANG, XIANGTING DONG*, WENSHENG YU, GUIXIA LIU
Key Laboratory of Applied Chemistry and Nanotechnology at Universities of Jilin Province, Changchun University of Science and Technology, Changchun 130022, P.R. of China

Fe_3O_4 nanofibers and nanoribbons have been successfully prepared by the combination of electrospinning and oxidation-reduction process. $Fe(NO_3)_3$/PVP nanofibers and nanoribbons were first fabricated by an electrospinning method. Subsequently, as-spun $Fe(NO_3)_3$/PVP nanocomposites have been stepwise transformed into Fe_2O_3 and Fe_3O_4 though an oxidation-reduction process. The obtained Fe_3O_4 nanofibers have an average diameter of about 120 nm and a large length to diameter ratio, and the Fe_3O_4 nanoribbons possess a width of ca. 3.44 μm and a thickness of ca. 49.2 nm, respectively. The saturation magnetizations of the Fe_3O_4 nanofibers and nanoribbons are 73.53 and 91.61emu·g^{-1}, respectively.

(Received May 26, 2013; accepted November 7, 2013)

Keywords: Electrospinning, Ferroferric oxide, Nanofiber, Nanoribbon

1. Introduction

Magnetic nanomaterials have attracted a lot of interest in recent years owing to their potential applications, such as biomacromolecules separation, catalyst separation, drug/gene delivery and release, and magnetic resonance imaging [1-3]. Therefore many traditional chemical methods have been applied to fabricate nano-sized ferroferric oxide materials, including precipitation [4], sol-gel [5], micro-emulsion [6], hydrothermal, solvothermal [7], and thermal decomposition methods [8]. Although various morphologies of nanoferroferric oxide have been obtained such as nanoparticles [9], nanorods [10], nanowire [11], nanofilm [12], nanocube, nanoctahedron, nanoctodecahedron, and nanododecahedron [13-15], it is difficult to prepare the nanofiber with a large length to diameter ratio via these traditional methods.

Electrospinning is a fascinating technique to process viscous solutions or melts into continuous fibers with diameters ranging from micrometer to submicron or nanometer. Therefore, it is applied in many areas such as filtration [16], optical and chemical sensors [17], biological scaffolds [18], electrode materials [19], and nanocables [20]. However, there are no reports on the preparation of ferroferric oxide nanofibers and nanoribbons through electrospinning or other routes.

Herein we report the preparation of the Fe_3O_4 nanofibers and nanoribbons via electrospinning technology and post-heat treatment. Meanwhile, we obtained α-Fe_2O_3 nanofibers and nanoribbons in the calcination process with different experimental conditions. The formation processes of the products were also investigated in detail.

2. Experimental

2.1 Chemicals

The starting chemical reagents were Poly vinylpyrrolidone (PVP, Mw≈90,000), N, N-dimethyl formamide (DMF) and $Fe(NO_3)_3·9H_2O$. All of chemicals were of analytical grade and directly used as received without further purification.

2.2 Preparation of precursor solution

A certain amount of $Fe(NO_3)_3·9H_2O$ was dissolved in 10g of DMF to form uniform solution under vigorous stirring at room temperature. Then a given mass of PVP was added into the above mixture solution and stirred for 12h. The actual mixture ratios were shown in Table 1.

Table 1. Compositions of the precursor solutions.

Compositions / Samples	DMF/g	PVP/g	$Fe(NO_3)_3·9H_2O$/g
$Fe(NO_3)_3$/PVP nanofiber	10.0	1.8	1.0
$Fe(NO_3)_3$/PVP nanoribbon	10.0	3.6	1.0

2.3 Synthesis of Fe_3O_4 nanofibers and nanoribbons

$Fe(NO_3)_3$/PVP nanofibers and nanoribbons were first synthesized via electrospinning technology. In a typical electrospinning process, the precursor solution was loaded into a plastic syringe with a spinneret. A flat iron net was put about 14cm away from the spinneret as a fiber collector. A positive direct current (DC) was applied between the spinneret and the collector to generate a stable continuous PVP-based composite nanofiber. The nanofibers were fabricated when the voltage of DC was adjusted to 13kV and the angle between spinneret and horizon was fixed to 15°. The nanoribbons were prepared when the voltage of DC was fixed at 8kV and the spinneret was settled vertically. Next, the as-prepared $Fe(NO_3)_3$/PVP nanofibers and nanoribbons were oxidized in air at 650℃ for 4h in a furnace at the heating rate of 1℃/min. When the furnace was cooled naturally, the Fe_2O_3 nanofibers and nanoribbons were obtained. Finally, Fe_3O_4 nanofibers and nanoribbons were successfully prepared by the reduction of Fe_2O_3 nanofibers and nanoribbons in the mixed atmosphere of 5% H_2 and 95% N_2 at 450℃ for 2h in a vacuum tube furnace at the heating rate of 5℃/min, and then cooled naturally.

2.4 Characterization methods

The as-prepared Fe_2O_3 nanofibers, nanoribbons and the products undergone different reduction times in the atmosphere of 5% H_2 and 95% N_2 were identified by an X-ray powder diffractometer (XRD, Bruker D8 FOCUS) with Cu Kα radiation. The operation voltage and current were kept at 40kV and 20mA, respectively. The morphologies of $Fe(NO_3)_3$/PVP, Fe_2O_3 and Fe_3O_4 nanofibers and nanoribbons were observed by a field emission scanning electron microscope (FESEM, XL-30). The magnetic performance of Fe_3O_4 nanofibers and nanoribbons were measured by a vibrating sample magnetometer (VSM, MPMS SQUID XL). All the measurements were performed at room temperature.

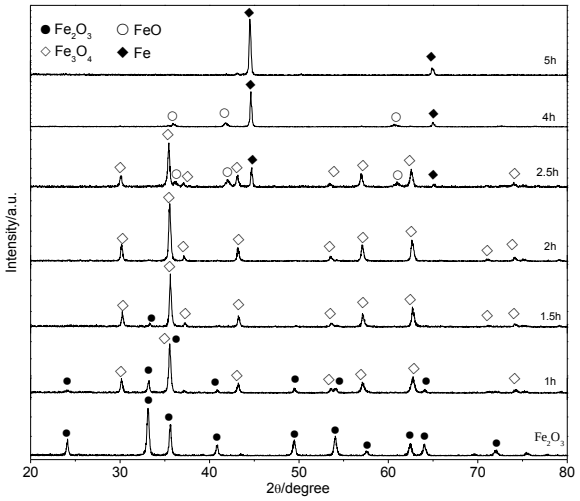

Fig. 1. XRD patterns of Fe_2O_3 nanofibers and the products undergone various reduction time in the mixed gases of 5% H_2 and 95% N_2.

3. Results and discussion

3.1 XRD analyses

Fig.1 shows the XRD patterns of Fe_2O_3 nanofibers and the products undergone various reduction time in the reducing atmosphere. It can be seen from Fig. 1 that pure phase α-Fe_2O_3 nanofibers were obtained after calcining the original fibers. All the peaks were found to match well with those of rhombohedral Fe_2O_3 [space group: R-3c] with cell constants a=b=5.036Å, c=13.746Å (PDF#33-0664). As the reduction time was prolonged in the reducing atmosphere, the α-Fe_2O_3 nanofibers were gradually converted to Fe_3O_4 nanofibers. Fe_3O_4 was formed when the reduction time was 1h and 1.5h. When the reduction time reached up to 2h, all the peaks could be readily identified as the pure cubic phase [space group: Fd-3m] of Fe_3O_4 with cell constants a=8.396Å (PDF#74-0748). No impurity peak was observed, indicating that the purity Fe_3O_4 nanofibers were successfully synthesized. With the further prolongation of reduction time, the main peak of Fe_3O_4 (2θ=35.4°) became weak and disappeared, while the diffraction peaks of FeO (2θ=41.9°, PDF#06-0615) and Fe (2θ=44.7°, PDF#06-0696) could be identified when the reduction time was 2.5h and 4h. When reaction time reached up to 5h, pure phase Fe nanofibers were obtained. Similar results were also observed in the Fe_3O_4 nanoribbon formation process. The relevant reaction equations are listed below:

$$Fe(NO_3)_3/PVP+O_2 \xrightarrow[4h]{650℃} CO_2+H_2O+NO_2+Fe_2O_3 \quad (1)$$

$$Fe_2O_3+H_2 \xrightarrow[2h]{450℃} H_2O+Fe_3O_4 \quad (2)$$

$$Fe_2O_3+H_2 \xrightarrow[5h]{450℃} H_2O+Fe \quad (3)$$

3.2 SEM analyses

Fig. 2 (a) shows SEM image of $Fe(NO_3)_3$/PVP nanofibers directly fabricated by electrospinning. Their diameters were 130±10 nm, and surface was smooth. Fig. 2 (b) gives the SEM image of the α-Fe_2O_3 nanofibers obtained from calcining $Fe(NO_3)_3$/PVP nanofibers at 650℃. Their diameters were 121±15 nm, which were relatively thinner than that of $Fe(NO_3)_3$/PVP nanofibers because of the decomposition of PVP. Fig 2 (c) illustrates the SEM image of the Fe_3O_4 nanofibers produced by the reduction of the α-Fe_2O_3 nanofibers in the atmosphere of 5% H_2 and 95% N_2 for 2h at 450℃. Their morphology was similar to that of α-Fe_2O_3 nanofibers, and the diameter was 120±18nm. Obviously, all the obtained nanofibers had a large length to diameter ratio. The α-Fe_2O_3 and Fe_3O_4 nanofibers were consisted of nanoparticles.

Fig. 2 (d) exhibits the SEM image of $Fe(NO_3)_3$/PVP nanoribbons obtained by direct electrospinning. The nanoribbons have a smooth surface with a width of ca. 13.35μm and a thickness of ca. 139 nm. Fig. 2 (e) reveals that the α-Fe_2O_3 nanoribbons have a width of ca. 3.45μm, and a thickness of ca. 51.1nm. It could be seen that a large number of holes were scattered on the α-Fe_2O_3 nanoribbons. Fig. 2 (f) gives the SEM image of the Fe_3O_4 nanoribbons. Their morphology is similar to that of the α-Fe_2O_3 nanoribbons, and their width and thickness are ca. 3.44μm and 49.2nm, respectively.

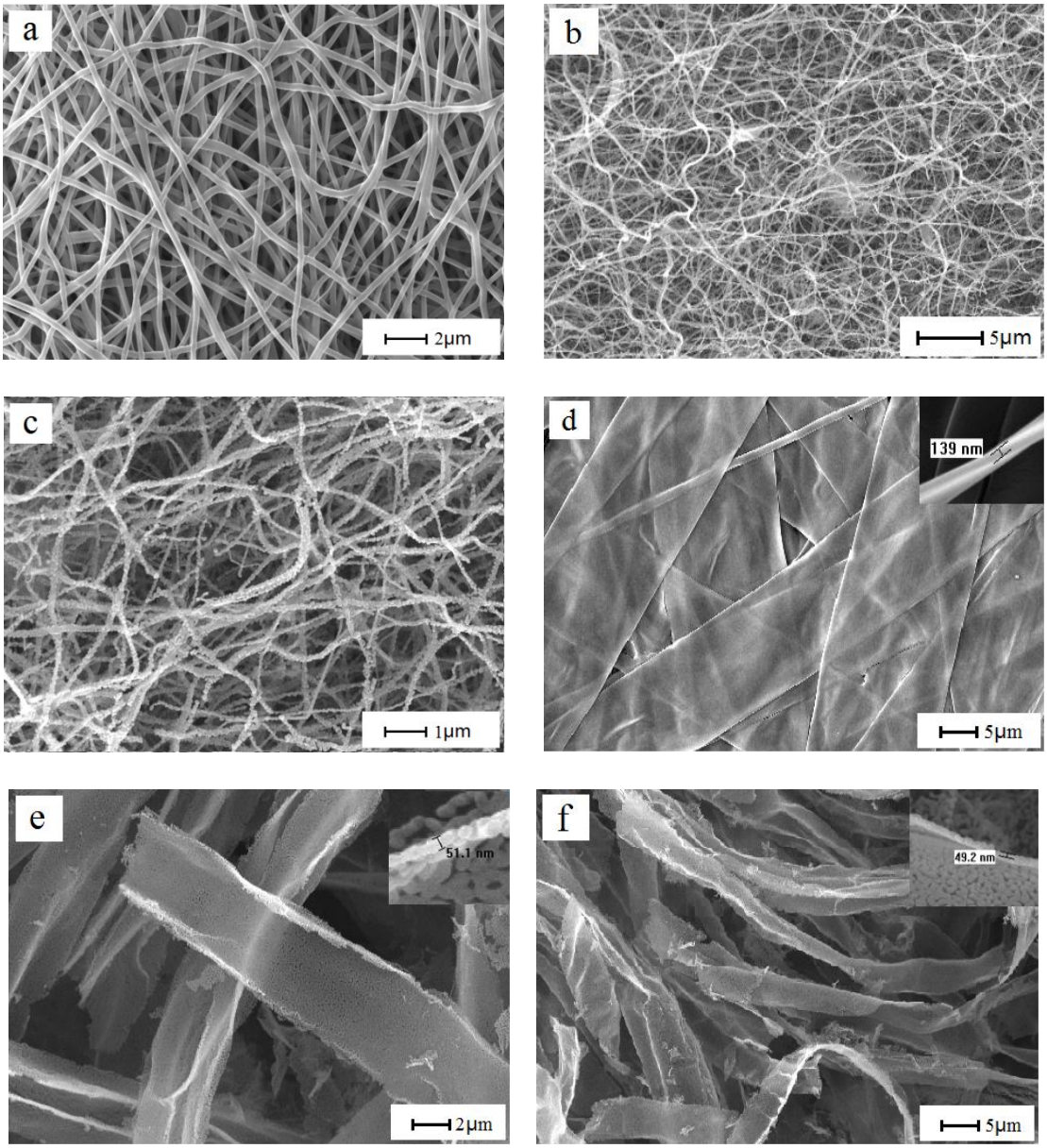

Fig. 2. SEM images of $Fe(NO_3)_3$/PVP nanofibers (a), Fe_2O_3 nanofibers (b), Fe_3O_4 nanofibers (c) and $Fe(NO_3)_3$/PVP nanoribbons (d), Fe_2O_3 nanoribbons (e), Fe_3O_4 nanoribbons (f).

3.3 VSM analyses

The magnetic properties of the Fe_3O_4 nanofibers and nanoribbons were investigated with a vibrating sample magnetometer. Fig. 3 shows the hysteresis loops of the samples, and the obtained data are summarized in Table 2. The saturation magnetization of the Fe_3O_4 nanofibers and nanoribbons were 73.53 and 91.61emu·g^{-1}, respectively. The remanence of the Fe_3O_4 nanofibers and nanoribbons were 25.14 and 32.96emu·g^{-1}, respectively. And the coercivities were 380.55 and 393.56Oe, respectively. These results indicate that the saturation magnetization,

remanence, and coercivity of the Fe_3O_4 nanoribbons were higher than those of the Fe_3O_4 nanofibers, which might result from the facts that Fe_3O_4 nanoribbons had bigger volume and smaller specific surface area, possessing fewer surface defects and more magnetic domains [21]. The obtained Fe_3O_4 nanofibers and nanoribbons behaved ferromagnetism due to the high-remanence and coercivity.

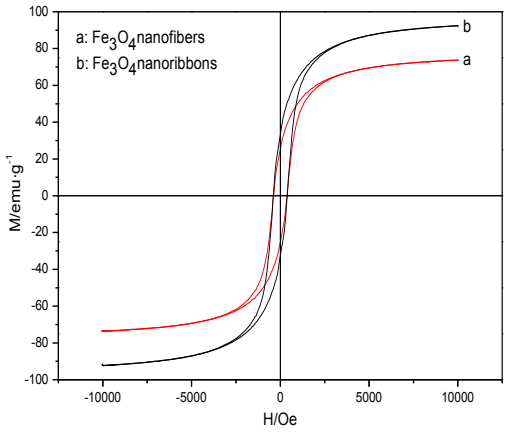

Fig. 3. Hysteresis loops of Fe_3O_4 nanofibers (a) and Fe_3O_4 nanoribbons (b).

Table 2. Magnetic Properties of Fe_3O_4 Nanofibers and Nanoribbons.

Items / Samples	Saturation magnetization (Ms)/emu·g^{-1}	Remanence(Mr) /emu·g^{-1}	Coercivity(Hc) /Oe	Mr/Ms
Fe_3O_4 nanofibers	73.53	25.14	380.55	0.342
Fe_3O_4 nanoribbons	91.61	32.96	393.56	0.360

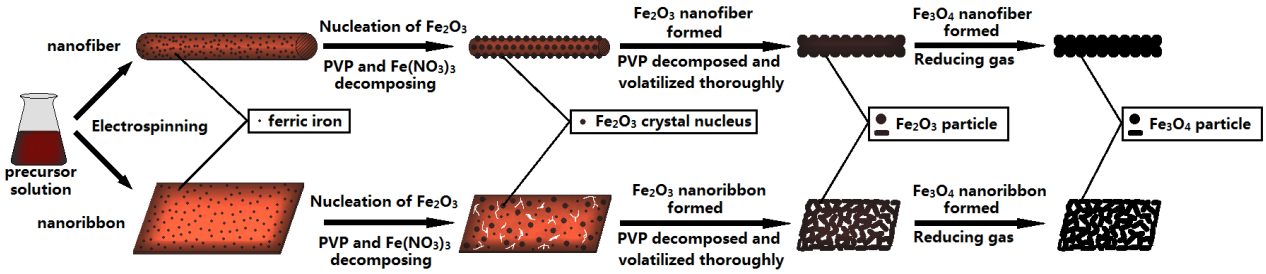

Fig. 4. Schematic diagram of formation mechanism of Fe_3O_4 nanofibers and Fe_3O_4 nanoribbons.

3.4 Formation mechanism of Fe_3O_4 nanofibers and nanoribbons

Fig. 4 shows the schematic diagram of the formation mechanism of the Fe_3O_4 nanofibers and Fe_3O_4 nanoribbons. The electrospun $Fe(NO_3)_3$/PVP nanofibers and nanoribbons were scaffolded by PVP, and scattered with Fe^{3+}. Then Fe_2O_3 crystal nuclei were formed as the calcining temperature was reached up to the decomposition temperature of $Fe(NO_3)_3$. The Fe_2O_3 crystal nucleus merged the nearby Fe^{3+} and grew up. When the temperature reached up to the decomposition temperature of PVP, the grown up α-Fe_2O_3 crystal-chain took over the framework of PVP and Fe_2O_3 nanomaterials were formed until PVP was completely decomposed and volatilized. In this process, the nanoribbons would generate cracks and formed net-like structure. The morphology of the Fe_3O_4 nanofibers and nanoribbons were consistent with that of the α-Fe_2O_3 nanofibers and nanoribbons after the reduction process.

4. Conclusions

Fe_3O_4 nanofibers and nanoribbons were successfully obtained by electrospinning and post-heat oxidation-reduction treatments. The average diameter of the Fe_3O_4 nanofibers was 120nm. The width and thickness of the Fe_3O_4 nanoribbons were about 3.44μm, and 49.2 nm, respectively. The saturation magnetization of the Fe_3O_4 nanofibers and nanoribbons were 73.53 and 91.61emu·g^{-1}, respectively. The new high-performance Fe_3O_4 nanomaterials have potential applications in memory device, nanorobots, protein determination and target delivery of drug, etc.

Acknowledgments

This work was financially supported by the National Natural Science Foundation of China (NSFC 50972020, 51072026), Ph.D. Programs Foundation of the Ministry of Education of China (20102216110002, 20112216120003), the Science and Technology Development Planning Project of Jilin Province (Grant Nos. 20130101001JC, 20070402, 20060504), the Science and Technology Research Project of the Education Department of Jilin Province during the eleventh five-year plan period (Under grant No. 2010JYT01), Key Research Project of Science and Technology of Ministry of Education of China (Grant No. 207026).

References

[1] M. Stein, J. Wieland, P. Steurer, F. Tölle, R. Mülhaupt, B. Breit, Adv. Synth. Catal., **353**, 523 (2011).
[2] F. H. Chen, L. M. Zhang, Q. T. Chen, Y. Zhang, Z. J. Zhang, Chem. Commun., **46**, 8633 (2010).
[3] H. Tan, J. M. Xue, B. Shuter, X. Li, J. Wang, Adv. Funct. Mater., **20**, 722 (2010).
[4] S. Wu, A. Z. Sun, F. Q. Zhai, J. Wang, W. H. Xu, Q. Zhang, A. A. Volinsky, Mater. Lett., **65**, 1882 (2011).
[5] J. Xu, H. B. Yang, W. Y. Fu, K. Du, Y. M. Sui, J. J. Chen, Y. Zeng, M. H. Li, G. T. Zou, J. Magn. Magn. Mater., **309**, 307 (2007).
[6] Vuthichai Ervithayasuporn, Yusuke Kawakami, J. Colloid Interface Sci., **332**, 389 (2009).
[7] G. X. Liu, H. X. Peng, J. X. Wang, X. T. Dong, J. Optoelectron. Adv. Mater. **14**, 205 (2012).
[8] X. H. Liu, Y. Guo, Y. G. Wang, J. W. Ren, Y. Q. Wang, Y. L. Guo, Y. Guo, G. Z. Lu, Y. S. Wang, Z. G. Zhi, J. Mater. Sci., **45**, 906 (2010).
[9] H. Deng, X. L. Li, Q. Peng, X. Wang, J. P. Chen, Y. D. Li, Angew. Chem. Int. Ed., **44**, 2782 (2005).
[10] W. Zhang, S. Y. Jia, Q. Wu, J. Y. Ran, S. H. Wu, Y. Liu, Mater. Lett., **65**, 1973 (2011).
[11] L. Y. Zhang, Y. F. Zhang, J. Magn. Magn. Mater., **321**, L15 (2009).
[12] Ali Erdem Eken, Macit Ozenbas, Sol-Gel Sci. Technol., **50**, 321 (2009).
[13] X. G. Yu, K. Z. Chen, Mater. Sci. Eng., **176**, 750 (2011).
[14] L. J. Zhao, H. J. Zhang, J. K. Tang, S. Y. Song, F. Cao, Mater. Lett., **63**, 307 (2009).
[15] L. F. Duan, S. S. Jia, Y. J. Wang, J. Chen, L. J. Zhao, J. Mater. Sci., **44**, 4407 (2009).
[16] Wannes Sambaer, Martin Zatloukal, Dusan Kimmer, Chem. Eng. Sci., **66**, 613 (2011).
[17] J. M. Corres, Y. R. Garcia, F. J. Arregui, I. R. Matias, IEEE Sens. J., **11**, 2383 (2011).
[18] S. A. Sell, P. S. Wolfe, J. J. Ericksen, D. G. Simpson, G. L. Bowlin, Tissue Eng. Part A, **17**, 2723 (2011).
[19] S. L. Chen, H. Q. Hou, F. Harnisch, S. A. Patil, A. A. Carmona-Martinez, S. Agarwal, Y. Y. Zhang, S. Sinha-Ray, A. L. Yarin, A. Greiner, U. Schröder, Energy Environ. Sci., **4**, 1417 (2011).
[20] C. Song, X. T. Dong, Optoelectron. Adv. Mater. Rapid Commun. **6**, 319 (2012).
[21] Toshihiko Sato, Tetsuo Iijima, Masahiro Seki, Nobuo Inagaki, J. Magn. Magn. Mater., **65**, 252 (1987).

*Corresponding author: dongxiangting888@163.com